Journal of Solid State Chemistry **167,** 412–419 (2002)
doi:10.1006/jssc.2002.9643

X-Ray and Electron Microscopy Studies of Rare-Earth Tungsten Bronzes

Carl Grenthe and Margareta Sundberg[1]

Department of Inorganic Chemistry, Arrhenius Laboratory, Stockholm University, S-106 91 Stockholm, Sweden

Received January 31, 2002; in revised form April 26, 2002; accepted May 3, 2002

Rare-earth tungsten bronzes, RE_xWO_3, of perovskite tungsten-bronze (PTB) type, formed by conventional solid-state synthesis, have been studied by X-ray powder diffraction, electron diffraction in combination with microanalysis, and high-resolution transmission electron microscopy (HRTEM). The X-ray patterns indicated cubic PTB type structure with $a \approx 3.83$ Å (subcell), while the electron microscopy study indicated a lowering of the subcell symmetry and a complex superstructure. The upper phase composition limit, $x \leq 0.25$, for the RE_xWO_3 bronzes with PTB-related structures was established from the microanalysis study. Ordered, disordered and microtwinned superstructures were revealed by electron diffraction patterns and HRTEM images taken along $\langle 110 \rangle_p$. The superstructure is due to filling of the interstices in the WO_3 structure with the rare-earth ions. A hypothetical model of the superstructure based on the contrast features in the HRTEM images has been deduced. The relationships between the RE_xWO_3 bronzes formed by solid-state synthesis under high- and ambient-pressure conditions are presented. © 2002 Elsevier Science (USA)

Key Words: **tungsten bronzes; HRTEM; electron diffraction; Superstructure; X-ray diffraction; microanalysis; rare-earth tungsten oxides; perovskites.**

INTRODUCTION

Tungsten bronzes are non-stoichiometric reduced compounds with the general formula A_xWO_3, where the A ion is an electropositive metal such as an alkali, alkaline-earth or rare-earth metal, and $0 < x < 1$. These substances have received much attention over the years because of their interesting physical and chemical properties such as metallic or semimetallic conductivity and a high inertness to most acids.

The rare-earth tungsten bronzes, $RE_{0.1}WO_3$ with RE = Ce–Lu, prepared by conventional solid-state synthesis, have been reported by Ostertag (1). Their structures were found to be of perovskite tungsten-bronze (PTB) type with cubic unit cells ($a \approx 3.8$ Å). The homogeneity range of the cubic Eu_xWO_3 and Gd_xWO_3 bronzes were investigated, and the X-ray results showed that PTB structures with cubic symmetry were formed in the region $0.085 \leq x \leq 0.16$, whereas a tetragonal phase was observed for low values of x ($x \leq 0.085$). Dimbylow et al. have later found that the cubic Eu_xWO_3 bronzes are stable in the region $0.085 \leq x \leq 0.125$ and that a tetragonal phase with the lattice parameters $a = 5.295$ Å and $c = 3.871$ Å exists at $x = 0.05$ (2). The solid-state synthesis method has also been used in a phase analysis study of the Nd_2O_3–WO_3–W system (3). X-ray analysis studies of a large number of multiphase samples showed that a cubic "bronze" phase of composition Nd_xWO_y, with $0.0606 \leq x \leq 0.154$ and $2.636 \leq y \leq 2.846$ was formed within a broad region of the subsystem $Nd_2W_3O_{12}$–WO_2–WO_3. The crystal structure of the PTB bronze $La_{0.14}WO_3$ has been determined from powder neutron diffraction data by Wiseman and Dickens (4). The results showed that $La_{0.14}WO_3$ has a simple cubic perovskite tungsten-bronze structure ($a \approx 3.8$ Å) without tilt of the WO_6 octahedra and with random distribution of the lanthanum atoms in the square tunnels. No superstructure reflections that would indicate a larger unit cell were observed.

Syntheses of tungsten bronzes at lower temperatures (<900°C) by means of thermal degradation of polyoxotungstates have recently been reported by Wasserman *et al.* (5). They found from X-ray analysis studies of the products that a cubic tungsten bronze of cerium (III), Ce_xWO_3, was formed for $x = 0.066$–0.162.

During the last few years we have been interested in exploring the influence of synthesis method and experimental conditions such as pressure and temperature on the formation and stability of the rare-earth tungsten oxide structures in the system $RE_2W_2O_9$–WO_3–WO_2. Our high-pressure synthesis experiments have shown that RE_xWO_3 bronzes with structures related to PTB, hexagonal tungsten bronze (HTB), and intergrowth tungsten bronze (ITB) can

[1]To whom correspondence should be addressed. Fax: 46-8-152187. E-mail: marsu@inorg.su.se, kalle@inorg.su.se.

0022-4596/02 $35.00

be prepared in the pressure region $P = 25$–50 kbar. It is noteworthy that the PTB bronzes were observed in samples synthesised at $P = 25$–30 kbar and $T > 1500$ K (6–9). Recent thermal analysis studies in argon atmosphere have shown that the HTB-related phase is metastable and transforms to a stable PTB-type structure and WO_3 (9). The TG experiments also showed that additional oxygen atoms were present in the HTB structure.

It is well established that the RE_xWO_3 bronzes formed by conventional solid-state synthesis have structures of PTB type, but there is still some uncertainty concerning the homogeneity region of the PTB bronzes, and their microstructures have not yet been characterized. The structural differences between the bronzes formed under high- and ambient-pressure conditions also suggested that a microstructural study focused on the RE_xWO_3 bronzes with PTB-type structures would be of interest. We thus found it worthwhile to reinvestigate the RE_xWO_3 system, especially for $0.1 \leq x \leq 0.3$, using a combination of X-ray powder diffraction and electron microscopy methods. The electron diffraction and high-resolution transmission electron microscopy (HRTEM) studies revealed the existence of a complex microstructure, which could be ordered, disordered or twinned depending on the distribution of the rare-earth ions on the voids in the WO_3 structure. The results are reported below and compared with those obtained of the high-pressure tungsten bronzes.

EXPERIMENTAL

Samples of composition RE_xWO_3, with $0.1 \leq x \leq 0.4$, were prepared by a solid-state reaction from appropriate amounts of RE_2O_3 with RE = La, Nd, Tb and Dy, CeO_2, WO_3 and W-metal powder. The starting materials were mixed as slurry in *n*-hexane for 2–3 h and, after removing the *n*-hexane, the resulting dry powders were heated in evacuated silica tubes at 1200–1300 K for 2–4 days. After cooling, the products were ground in an agate mortar and heated again in the same manner.

X-ray powder diffraction photographs of all samples were taken in a subtraction-geometry Guinier–Hägg focusing camera with strictly monochromatized Cu$K\alpha_1$ radiation. Silicon was added as internal 2θ standard. The photographs were measured with an automatic microdensitometer (10), and the positions of the silicon lines were used to correct for sample displacement, zero-point error and film shrinkage. Finally, the X-ray powder patterns were indexed and the unit-cell parameters refined with the program PIRUM (11).

The samples were characterized by energy-dispersive X-ray spectroscopy (EDS), using the scanning electron microscopes JEOL 820 and JEOL 880. The first one is equipped with a LINK AN10000 EDS system and the latter with an attached LINK ISIS EDS system (GE detector). The TEM specimens were prepared by crushing a small amount of the sample in an agate mortar and then suspending it in *n*-butanol. A drop of this suspension was placed on a perforated carbon film supported on a copper grid. The phase composition and structure type were investigated by combining selected-area electron diffraction (SAED) and EDS microanalysis studies of the same crystal fragments in a JEOL JEM 2000FX-II transmission electron microscope, equipped with LINK AN10000 EDS microanalysis system. The ordered and defect structures were investigated by high-resolution transmission electron microscopy (HRTEM). The HRTEM images were taken in a JEOL JEM 3010 operated at 300 kV accelerating voltage, equipped with a double-tilt, side-entry goniometer stage with maximum tilt angles of ± 10–20^0. Electron diffraction patterns were simulated with an upgraded version of the program DIFPAT (12), and theoretical HRTEM images were calculated using a locally modified PC version of the SHRLI suite of programs (13).

RESULTS

The colors of the RE_xWO_3 samples were almost always dark blue to black with a metallic lustre, which is typical of slightly reduced binary tungsten oxides and tungsten bronzes. The products were microcrystalline and showed no signs that the crystals had started to melt.

Most of the X-ray powder patterns contained many diffraction lines, which indicated that two- or multi-phase samples were formed. Peaks characteristic of a PTB bronze with a cubic unit-cell ($a \approx 3.8$ Å) could be identified in all photographs. The unit-cell dimensions, refined from the corresponding X-ray data, are given in Table 1. The X-ray patterns indicated that most of the samples with $x \leq 0.15$ contained a small amount of WO_3. Lines characteristic of the rare-earth tungstate $RE_2(WO_4)_3$ were observed in the X-ray data from samples with $x \geq 0.2$. The latter patterns also revealed that the amount of the tungstate increased with increasing x value of the bulk material. A few weak lines observed in the photographs of $RE_{0.3}WO_3$ and $RE_{0.4}WO_3$ could be assigned to WO_2. It is noteworthy that diffraction lines of the rare-earth tungstate $RE_{10}W_{22}O_{81}$ could not be seen in the X-ray records from the samples with $x \geq 0.2$. The results from the phase analysis study are summarized in Table 1. From the intensity of the lines in the X-ray powder patterns, the upper composition limit for the RE_xWO_3 bronzes of PTB type seems to be in the range $x = 0.2$–0.3 in the investigated temperature region 1200–1300 K.

Two almost pure PTB-bronze samples have been prepared, $La_{0.15}WO_3$ and $Nd_{0.20}WO_3$. The diffraction lines in the X-ray pattern of $La_{0.15}WO_3$ were rather broad, and all reflections above $2\theta = 70^\circ$ showed a very small splitting into doublets, thus indicating either lowering of symmetry

TABLE 1
X-Ray and Electron Microscopy Results of RE_xWO_3 Bulk Samples

Bulk sample		RE_xWO_3 (PTB)-related structures					
		SEM/EDS		TEM/EDS		XRD	
RE	*x*	*x*-range	Mean	*x*-range	Mean	Unit cell	Additional compounds
La	0.10	0.07 – 0.14	0.11			3.8218(1)	WO_3
	0.15	0.09 – 0.13	0.12	0.08 – 0.15	0.11	$a = 3.837$ $c = 3.832$	
	0.20	0.11 – 0.16	0.13			3.8326(4)	$La_2(WO_4)_3$, $La_{10}W_{22}O_{81}^{ED}$
	0.25	0.11 – 0.22	0.18	0.11 – 0.19	0.16	3.8295(4)	$La_2(WO_4)_3$, WO_2^{XRD}, $La_{10}W_{22}O_{81}^{ED}$
Ce	0.20					3.8223(3)	WO_3, $Ce_{10}W_{22}O_{81}^{ED}$
	0.30	0.11 – 0.21	0.15	0.15 – 0.17	0.16	3.8360(3)	$Ce_2(WO_4)_3$, WO_2^{XRD} ,$Ce_{10}W_{22}O_{81}^{ED}$
Nd	0.10	0.05 – 0.09	0.07	0.05 – 0.10	0.06	3.8243(1)	WO_3
	0.15	0.08 – 0.13	0.11			3.8254(2)	WO_3
	0.20	0.13 – 0.20	0.15	0.11 – 0.23	0.19	3.8316(3)	$Nd_{10}W_{22}O_{81}^{ED}$
	0.30	0.12 – 0.22	0.17	0.16 – 0.24	0.20	3.8397(3)	$Nd_2(WO_4)_3$, WO_2^{XRD}, $Nd_{10}W_{22}O_{81}^{ED}$
	0.40	~0.18				3.8335(3)	$Nd_2(WO_4)_3$, WO_2^{XRD}
Tb	0.15	0.06 – 0.14	0.11	0.11 – 0.14	0.12	3.8116(1)	WO_3
	0.20	0.08 – 0.16	0.13	0.10 – 0.17	0.13	3.8105(1)	$Tb_2(WO_4)_3$
	0.30	0.10 – 0.15	0.11	0.10 – 0.16	0.14	3.8107(1)	$Tb_2(WO_4)_3$, WO_2^{XRD}
Dy	0.15	0.06 – 0.11	0.07	0.06 – 0.10	0.07	3.8066(1)	WO_3
	0.20	0.06 – 0.16	0.11	0.12 – 0.16	0.14	3.8067(1)	$Dy_2(WO_4)_3$
	0.25	0.12 – 0.19	0.16	0.11 – 0.19	0.15	3.8093(2)	$Dy_2(WO_4)_3$, WO_2^{XRD}

Note. XRD Compounds identified only from the X-ray diffraction pattern. ED, Compounds identified only from ED/EDS studies.

of the PTB bronze structure or the presence of more than one phase. The X-ray results in Table 2 show that the reflections could be indexed with a tetragonal unit cell with $c/a = 0.9985$. The broad peaks indicated that a cubic PTB bronze could also be present in the sample.

The microanalysis studies of 25–50 crystallites from each sample in the SEM and TEM microscopes largely confirmed the results from the X-ray diffraction study, as can be seen from Table 1. The SEM/EDS and ED/EDS investigations also revealed the presence of a few crystals of $RE_{10}W_{22}O_{81}$ in the La, Ce and Nd samples with $x = 0.2$ and 0.3. The *RE* bronze with a PTB-related structure was the only compound of variable composition, and the *x* value in RE_xWO_3 was found to vary between 0.05 and 0.25. Table 1 shows that the *RE* content in the crystals increased with increasing amount of rare earth in the starting material, up to a value of $x \approx 0.20$. Only a few fragments with $x = 0.20$–0.25 have been observed in samples of bulk composition $RE_{0.2}WO_3$ and $RE_{0.3}WO_3$. The latter bulk compositions seem to favor the formation of the $RE_{10}W_{22}O_{81}$ and $RE_2(WO_4)_3$ tungstates, which both seemed to be essentially stoichiometric according to the ED/EDS results.

The X-ray and ED/EDS results also indicate a probable relationship between the *RE* content in the PTB crystals and the length of the *a*-axis. For example, when the average Nd content in the PTB crystals from the five Nd samples in Table 1 increases from $x = 0.06$ to 0.20, the length of *a* increases from 3.8243 to 3.8397 Å. It can also be seen from the EDS results that the *a*-axis of the cubic unit cell decreases from $Ce_{\sim 0.15}WO_3$ ($a = 3.8360$ Å) to $Dy_{\sim 0.15}WO_3$ ($a = 3.8093$ Å), in agreement with the lanthanide contrac-

TABLE 2
X-Ray Powder Data for $La_{0.15}WO_3$

I_{obs}	d_{obs} (Å)	$Sin^2\Theta_{obs}$	$Sin^2\Theta_{calc}$	*hkl*
100.0	3.8369	0.040305	0.040297	100
73.07	2.7100	0.080796	0.080711	110
23.85	2.2137	0.121081	0.121008	111
93.04	1.7161	0.201476	0.201483	210
85.05	1.5665	0.241798	0.241897	211
26.82	1.3553	0.323037	0.322845	202
17.13	1.2791	0.362499	0.362593	300
41.76	1.2773	0.363520	0.363724	003
20.43	1.2126	0.402893	0.402958	310
30.23	1.2111	0.403928	0.404020	103
7.14	1.1550	0.443428	0.443372	311
10.17	1.1536	0.444516	0.444316	113

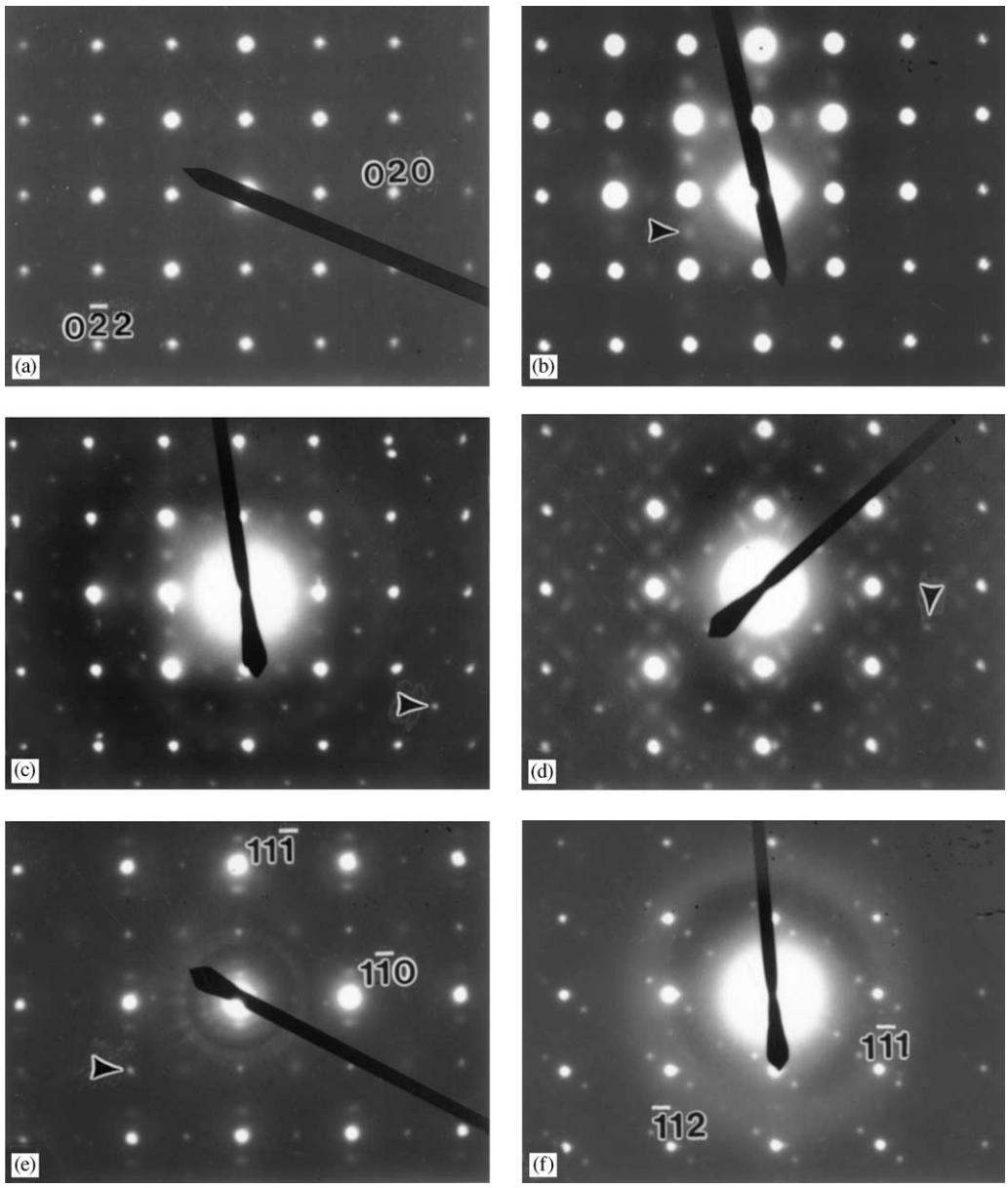

FIG. 1. Selected-area electron diffraction patterns of thin crystallites from the bulk samples RE_xWO_3: (a) $Dy_{0.2}WO_3$ along $[100]_p$; (b) $La_{0.2}WO_3$ along $[100]_p$; (c) $Tb_{0.2}WO_3$ along $[100]_p$; (d) $Tb_{0.2}WO_3$ along $[110]_p$; (e) $Tb_{0.2}WO_3$ along $[112]_p$; and (e) $Tb_{0.2}WO_3$ along $[110]_p$.

tion, and this confirms previous X-ray observations by Ostertag (1).

A large number of ED patterns have been taken of RE_xWO_3 crystals in different orientations, and some examples are shown in Fig. 1a–f. Two types of superlattice reflections are seen in these patterns. The first type of weak superlattice spots can be assigned to the basic WO_3 structure; these reflections indicate a doubling of the unit cell dimensions and a lowering of symmetry from cubic, as previously reported for the ideal PTB bronze structure of $La_{0.14}WO_3$ (4). The second type of superlattice reflections can be linked to the distribution of rare-earth ions in the voids of the WO_3 structure. The ED patterns in Fig. 1a–1c are all taken from PTB-type crystals aligned along $[100]_p$, with p referring to the basic cubic unit cell (subcell) with $a_p \approx 3.8$ Å. Figure 1a shows only the subcell spots, whereas the additional weak reflections along $[010]_p$ and $[001]_p$ in Fig. 1b and in the center of the squares in Fig. 1c suggest a doubling of the subcell parameters $a \approx b \approx c \approx 2 \times a_p$. These reflections are too weak to show up in the X-ray powder patterns. The ED patterns in Fig. 1b and c are also very similar to those of the monoclinic modification of WO_3,

but microanalysis studies confirm an *RE* content of $x = 0.18$–0.20 in the examined crystals. The Tb_xWO_3 crystal used for Fig. 1c was tilted about 45° around c^*, and the resulting ED pattern in $[110]_p$ projection is shown in Fig. 1d. Further tilt of the crystal resulted in the $[112]_p$ zone-axis pattern in Fig. 1e. The weak spots marked by arrows support the assumption that the true subcell parameters are doubled ($2 \times a_p$). The diffuse, streaked, closely spaced superlattice reflections along the two diagonals of reciprocal cell in Fig. 1d indicate the presence of a superstructure which is frequently twinned with a mirror normal to c^*. The spacing between the superlattice spots in the ED-patterns in Fig. 1d and e corresponds to a distance of about 12 Å in the structure. The ED pattern in Fig.1f ($\langle 110 \rangle_p$ zone), which was obtained from a few RE_xWO_3 crystals only, represents an untwinned pattern of a superstructure of lattice dimensions $a \approx 4.6$ Å, $b \approx 5.4$ Å (projection axis), $c \approx 12.2$ Å and $\beta \approx 105°$. The superlattice reflections suggest that the rare-earth ions are located in planes parallel to $\{111\}_p$, with a distance of about 12 Å between the planes in the WO_3 structure. A large number of ED patterns similar to that in Fig. 1d have been taken of thin crystallites from the RE_xWO_3 samples with $x \geq 0.15$. Microanalysis studies of these crystals showed that the *RE* content was in most cases in the range 0.15–0.20.

The HRTEM image of a thin crystal from the $La_{0.2}WO_3$ sample whose ED pattern is reproduced Fig. 1b is shown in Fig. 2. The network of dark dotted lines with a lattice spacing of 3.8 Å represents the projected framework of corner-sharing WO_6 octahedra. The white dots correspond to empty or almost empty tunnels, and the larger black dots marked by arrows indicate the presence of La^{3+} ions in the voids. The white fringe patterns with a periodicity of 7.5 Å (see arrows), which can be seen in microdomains oriented either along $[010]_p$ or $[001]_p$ are always visible in connection with the larger black dots. The fringes, which rarely cross each other, indicate that the symmetry of the WO_3 framework structure is affected by the location and the amount of La^{3+} ions in the tunnels and that the local symmetry of the framework is most likely orthorhombic or monoclinic, probably due to a slight tilt or distortion of the WO_6-octahedra in the neighborhood of the La^{3+} ions. The fringes are also visible in the corresponding SAED pattern as additional weak superlattice reflections. The SAED pattern exhibits the average symmetry of the examined crystallite, however, and not the local symmetry of the microdomain areas. The contrast features in the HRTEM image suggest that the La^{3+} ions locally prefer to enter every second or third tunnel. Short rows of two to four filled tunnels can be seen for example at A. However, it is not possible to obtain any information from the image about the location of the La^{3+} ions along the projection axis, but full occupancy of all sites along a tunnel row seems very unlikely because of the high charge of the La^{3+} ion and the low La content ($x \approx 0.10$–0.20) of the crystals.

The ED studies of thin crystal fragments from the RE_xWO_3 samples indicated that the $\langle 110 \rangle_p$ projections should be the most useful for studying the superstructure because the corresponding patterns frequently exhibit ordered, diffuse and streaked superlattice reflections, often in twinned orientations, as can be seen from Fig. 1d. Two typical HRTEM images are shown in Fig. 3; they both

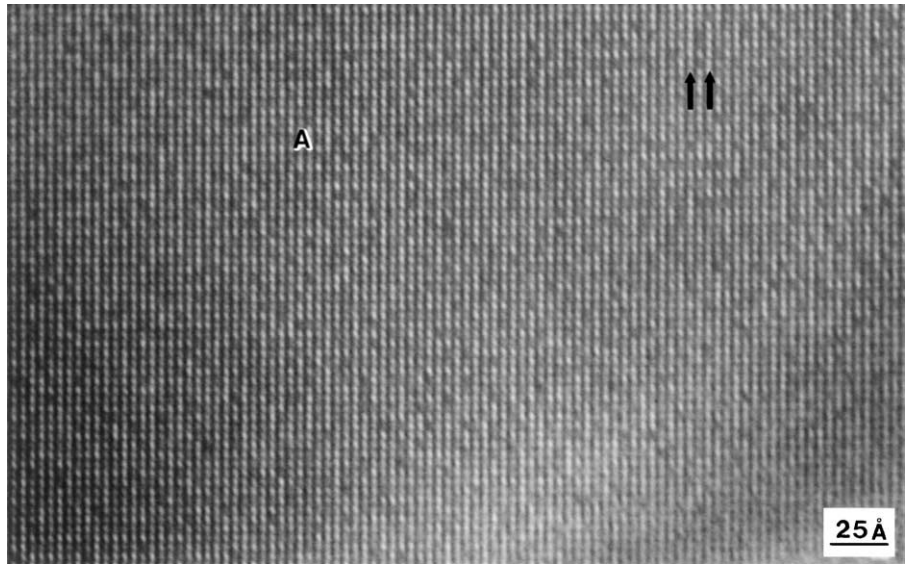

FIG. 2. HRTEM image ([100] zone) of a thin crystallite from the $La_{0.2}WO_3$ sample yielding the SAED pattern given in Fig.1b. The black dots show voids in the WO_3 structure, which are partly occupied by La^{3+} ions. Short rows of two to four filled tunnel sites can be seen at A.

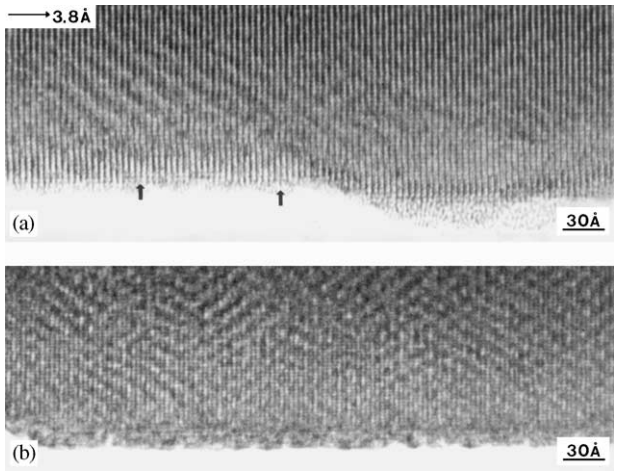

FIG. 3. HRTEM images in the $[110]_p$ projection, showing a fairly ordered superstructure of PTB type (a) and a twinned superstructure in microdomains in (b).

contain a rectangular network of dotted lines corresponding to the ideal WO_3 structure in the $[110]_p$ projection. The contrast features in Fig. 3a clearly show that the dotted lines normal to the 3.8 Å axis form a slightly wavy pattern (see arrows), which seems to be due to the location of RE^{3+} ions in the interstices of the WO_3 structure. The weak, diffuse, fairly straight bands of darker contrast in planes parallel to $\{111\}_p$ reveal the location of RE^{3+}. The HRTEM image in Fig. 3b, with the corresponding ED pattern in Fig. 1d, shows a twinned pattern of dark diffuse bands in microdomains. The image indicates that microtwinning is present in the crystal and that the twins are related by a mirror perpendicular to the 3.8 Å axis. The distance between the dark bands in Fig. 3a and b is in the range 12–13 Å. A closer analysis of the diffuse bands indicates that RE^{3+} prefers to enter the WO_3 network in such a way that pairs of RE^{3+} ions are formed in the $\langle 110 \rangle_p$ projections, as seen in the idealized structure models in Fig.4, where the open circles represent the *RE* positions. The unit-cell dimensions of the superstructure are $a \approx 2 \times 4.6 = 9.2$ Å, $b \approx 5.4$ Å (projection axis), $c \approx 12.2$ Å and $\beta \approx 105^\circ$, in agreement with those calculated from the ED pattern in Fig. 1f. The composition of the superstructure model is $Nd_2W_{10}O_{30}$ ($Nd_{0.2}WO_3$) when the *RE* positions are 50% occupied. There is a random distribution of *RE* ions and vacancies on the *RE* sites in Fig. 4a, whereas the structure model in Fig. 4b shows an ordered arrangement of filled and empty *RE* positions. From the contrast features in the HRTEM images it is quite clear that there are local variations in the filling of the interstices of the WO_3 structure. The microanalysis results from a large number of crystals also showed that the available *RE* positions in most cases were less than half-filled ($x \leq 0.2$). Both proposed models in Fig. 4a and b and the twin model in Fig. 4c seem to be reasonable approximations, however.

Sets of simulated HRTEM images have been calculated on the basis of the two structure models in Fig. 4a and b, and some of these images are shown in Fig. 5a and b. The dark diffuse bands (a) and the diffuse spots (b) show the location of the RE^{3+} ions in the WO_3 structure. There is a fairly good agreement between the observed (Fig. 3) and calculated images (Fig. 5), which support the suggested models. From the contrast features in the HRTEM images it is clear that the diffuse bands are not as straight as in the simulated images, indicating that there are local variations (disorder) in the filling of the interstices. Compared with the black contrast features from the WO_3 framework structure, it is also apparent that the WO_6 octahedra are slightly distorted in the neighborhood of the RE^{3+} ions,

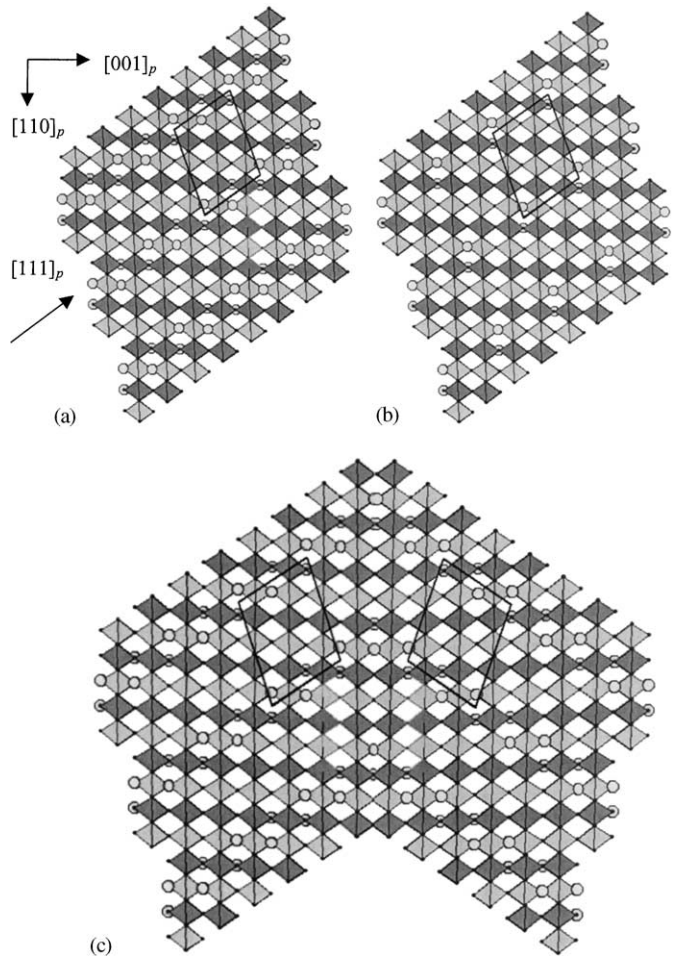

FIG. 4. Idealized model of the superstructure, deduced from the contrast features in the HRTEM images in Fig. 3. The open circles represent the *RE* positions. The *RE* sites are half-filled in (a) and fully occupied in (b). The idealized model of a twinned superstructure is shown in c) The unit cells are outlined. The models have been produced with ATOMS by Shape Software.

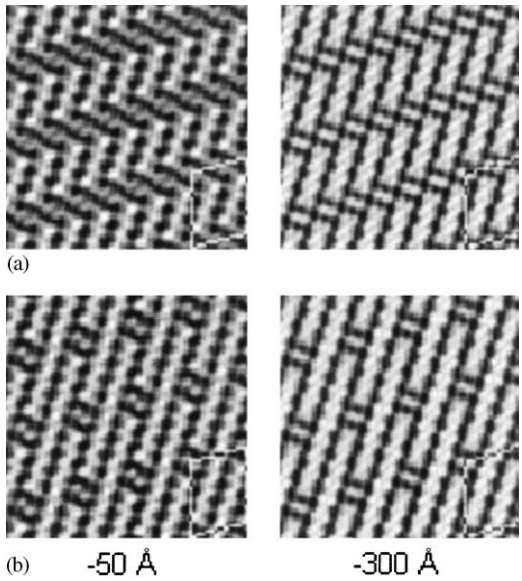

FIG. 5. (a) Two simulated images of the structure model in Fig. 4a. (b) Two simulated images of the structure model in Fig. 4b. The dark diffuse bands in (a) and the diffuse spots in (b) show the location of the *RE* ions in the structure. Crystal thickness ≈ 44 Å, Defocus values -50 Å and -300 Å.

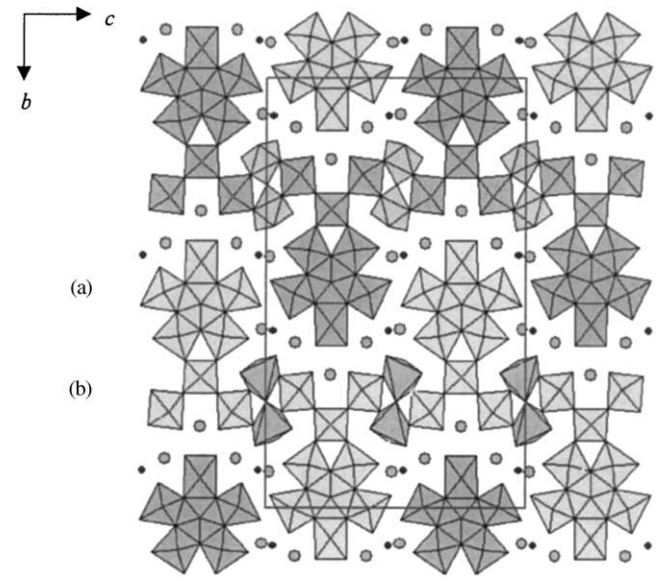

FIG. 7. The crystal structure of $Nd_{10}W_{22}O_{81}$ projected along the 3.8 Å axis. The two slabs of WO_3-related structure at $x = 0.25$ and 0.75 are denoted A and B, respectively. The Nd atoms are shown by filled dots. The unit cell is outlined.

since the black dotted lines are not as straight in the HRTEM images as in the simulated images.

In addition to the ordered, disordered and microtwinned superstructures, some isolated defects of another structure type have been seen in HRTEM images from PTB-type crystals containing terbium or dysprosium, and one example is demonstrated in the micrograph in Fig. 6. The right-hand part of the HRTEM image in the $[100]_p$ projection shows similar filling of the square tunnels with *RE* ions as previously demonstrated by Fig. 2. The two isolated faults perpendicular to each other in Fig. 6 can be described as consisting of alternating large black dots and white spots lined up along the $[012]_p$ and $[021]_p$ directions. The white dots indicate that larger tunnels, probably five- or six-sided, are present in the defect structure. The WO_3 structure is also heavily distorted in the neighborhood of the fault, and the network of corner-sharing WO_6 octahedra does not seem to be continuous across the fault. These features suggest that the large black dots might represent pentagonal columns (PCs) in the structure. The latter structure-building entity can be described as a pentagonal WO_7 bipyramid surrounded by five edge-sharing WO_6 octahedra, and these units are stacked one on top of the other and linked by corner sharing to form a PC (14). They can be found in the structures of the reduced binary oxides $W_{12}O_{34}$ (15) and $W_{18}O_{49}$ (16) and in the rare-earth tungstate $RE_{10}W_{22}O_{81}$ (17). The latter is shown in Fig. 7. A geometrical mechanism for the formation of a PC from six corner-sharing WO_6 octahedra in the WO_3 network has previously been reported (18). The contrast features from the faults in Fig. 6 resemble to some extent those from defects built up of PCs and six-sided tunnels, previously observed in HRTEM images of reduced tungsten oxides (18), intergrowth tungsten-bronzes (ITB) containing alkali [19], and the ITB bronzoids (20). The RE_xWO_3 samples in this study are all reduced, and with an increased *RE* content in the crystals the oxidation state of tungsten is decreased, so the observed defect might be a result of local reduction of tungsten.

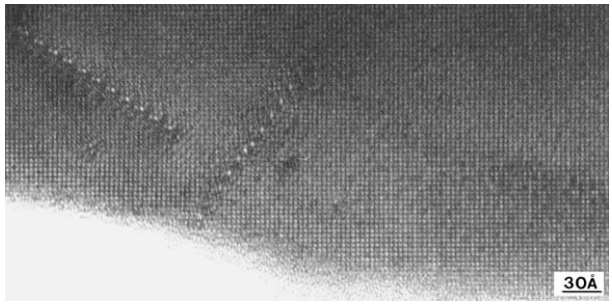

FIG. 6. HRTEM image of a PTB-type crystal from the $Dy_{0.2}WO_3$ sample projected along the 3.8 Å axis, showing isolated faults in a WO_3 type lattice.

STRUCTURAL RELATIONSHIP AND DISCUSSION

It was found from the X-ray diffraction study that a rare-earth tungsten bronze, RE_xWO_3, with a PTB-type

structure of cubic symmetry (subcell) was present in all samples. The HRTEM studies showed a lowering of the subcell symmetry, and the ED/EDS results also indicated that both the subcell symmetry and the unit-cell dimensions could differ between individual crystals. These factors are most likely due to the amount of rare-earth ions in the crystals and the accompanying local filling of the tunnel sites in the WO_3 network. The microanalysis results showed that the phase is stable for $x \leq 0.25$, which means that the filling of the interstices in the WO_3 structure is less than 25%. Previous studies on the Nd- and Eu-PTB bronzes have shown that the occupancy of the tunnel sites is $\leq 16\%$ (1, 2). A superstructure of the PTB bronze RE_xWO_3 is formed for $x = 0.15$–0.25. The proposed idealized superstructure model in Fig. 4 can be described as an ordered intergrowth of slabs parallel to $\{111\}_p$ of the PTB structure, three octahedra wide, and thin lamellas of WO_3, two octahedera wide, where the A site in the PTB slabs is partly occupied by *RE* ions.

Comparing the Na_xWO_3 and La_xWO_3 compounds, the sodium phase can have an x_{max} value almost $= 1$ ($x \leq 0.95$) (21), whereas the corresponding x_{max} value for the La phase is about $\frac{1}{4}$ of that. The RE^{3+} ions furthermore have a higher charge than Na^+, so if the charge were decisive one would expect the *RE* content to be $\frac{1}{3}$ of that of sodium. The observed maximum is still lower, though, so the limiting factor does not seem to be only the oxidation state of tungsten. If we assume that the WO_3 network is the same in both of these phases, the electrostatic repulsion force is nine times larger between two La^{3+} ions than between two Na^+ ions, using the lattice energy formula MZ^2/R. Therefore, it seems rather unfavorable for two La^{3+} ions to occupy two adjacent positions, so the six positions closest to every La^{3+} ion are probably empty.

The crystal structure of $Nd_{10}W_{22}O_{81}$ in Fig. 7, has some notable similarities with the PTB structure in the $\langle 100 \rangle_p$ projection. It is built up of thin WO_3-related slabs parallel to $[011]_p$ (marked A and B), which consist of WO_3-type fragments, three octahedra wide, linked to pairs of tilted octahedra (W_2O_{11} groups). The WO_3 fragments are also linked to PCs by corner sharing, as can be seen in Fig. 7. The WO_3-related slabs alternate at two levels, $x = 0.25$ and $x = 0.75$, along the *b*-axis. The *RE* atoms are arranged in a zigzag pattern in the space between the slabs, and they form the only link between the layers. The structure of $RE_{10}W_{22}O_{81}$ can be hypothetically considered as formed from the RE_xWO_3 bronze structure. The *RE* atoms have cracked open the WO_3 structure, splitting it into two layers that form the slabs described above.

It is noteworthy that RE_xWO_3 bronzes of PTB type can be prepared at high pressures under certain experimental conditions (22). For pressures below $P \leq 20$ kbar, only RE_xWO_3 bronzes of PTB type were formed, whereas both the pressure and the temperature have a significant influence on the phases formed in the region $P = 20$–50 kbar. If the pressure is increased, the temperature must also be increased for the formation of PTB bronzes. Moreover, the PTB bronzes prepared by solid-state synthesis under high- and ambient-pressure conditions have very similar structures and seem to differ only in the *RE* content.

ACKNOWLEDGMENTS

We thank Prof. Lars Kihlborg for valuable comments on the manuscript and Mrs. Jaroslava Östberg for technical assistance with the photographic work. This investigation forms a part of a research project financially supported by the Swedish Natural Science Research Council.

REFERENCES

1. W. Ostertag, *Inorg. Chem.* **5,** 758 (1965).
2. C. S. Dimbylow, I. J. McColm, C. M. P. Barton, N. N. Greenwood, and G. E. Turner, *J. Solid State Chem.* **10,** 128 (1974).
3. I. N. Belyaev and L. A. Voropanova, *Russ. J. Inorg. Chem.* **21,** 1713 (1976).
4. P. J. Wiseman and P. G. Dickens, *J. Solid State Chem.* **17,** 91 (1976).
5. K. Wassermann, M. T. Pope, M. Salmen, J. N. Dann, and H.-J. Lunk, *J. Solid State Chem.* **149,** 378 (2000).
6. N. D. Zakharov, Z. Liliental-Weber, V. P. Filonenko, I. P. Zibrov, and M. Sundberg, *Mater. Res. Bull.* **31,** 373 (1996).
7. N. D. Zakharov, P. Werner, I. P. Zibrov, V. P. Filonenko, and M. Sundberg, *J. Solid State Chem.* **147,** 536 (1999).
8. C. Grenthe, M. Sundberg, V. P. Filonenko, and I. P. Zibrov, *J. Solid State Chem.* **154,** 466 (2000).
9. V. P. Filonenko, C. Grenthe, M. Nygren, M. Sundberg, and I. P. Zibrov, *J. Solid State Chem.* **163,** 84 (2002)
10. K.-E. Johansson, T. Palm, and P.-E. Werner, *J. Phys. E* **13,** 1289 (1980).
11. P.-E.Werner, *Arkiv Kemi* **31,** 513 (1969).
12. A. J. Skarnulis, G. Liljestrand, and L. Kihlborg, *Chem. Commun. Univ. Stockholm* **1,** (1979).
13. M. A. O'Keefe, P. R. Buseck, and S. Iijima, *Nature* (London) **274,** 322 (1978).
14. M. Lundberg, *Chem. Commun. Univ. Stockholm* **12,** 1 (1971).
15. M. Sundberg, *Chem. Scripta* **14,** 161 (1978–79).
16. A. Magnéli, *Arkiv Kemi* **1,** 223 (1949).
17. C. Grenthe, A. Guagliardi, M. Sundberg, and P.-E. Werner, *Acta Crystallogr. B* **57,** 13 (2001).
18. W. Sahle and M. Sundberg, *Chem. Scripta* **16,** 163 (1980).
19. L. Kihlborg, M. Sundberg, and A. Hussain, *Chem. Scripta* **15,** 182 (1980).
20. R. Sharma, *Chem. Commun. Univ. of Stockholm* 3 (1985).
21. R. Clarke, *Phys. Rev. Lett.* **39,** 1550 (1977).
22. C. Grenthe, M. Sundberg, V. P. Filonenko, and I. P. Zibrov, *J. Solid State Chem.* submitted.